Hindawi
Mathematical Problems in Engineering
Volume 2022, Article ID 2082210, 14 pages
https://doi.org/10.1155/2022/2082210

Research Article

Influence Factors of Inherent Characteristics of F5 Cold-Rolling Mill's Main Drive System

Xingdou Jia, Xiaoqiang Yan, and Lidong Wang

School of Mechanical Engineering, University of Science and Technology Beijing, Beijing 100083, China

Correspondence should be addressed to Xiaoqiang Yan; yanxq@ustb.edu.cn

Received 15 July 2022; Revised 25 September 2022; Accepted 3 October 2022; Published 26 October 2022

Academic Editor: Francisco Beltran-Carbajal

This paper is focused on the inherent characteristics of the main drive system of the F5 cold-rolling mill in a steel plant. First, the main transmission mechanical structure was simplified to a five-inertia torsional vibration model. Secondly, the coupled torsional vibration model of strip and roll was established. The electromechanical coupling model of the motor control system and the motor rotor was established again. Finally, the AMESim software was used to calculate the natural frequency of the main drive system under various coupling conditions, and the influence mechanism of rolling parameters and motor control system parameters on the natural frequency of the main drive system was obtained, and an example of torsional vibration suppression is given by adjusting the control parameters. This study provides a profound theoretical basis for the on-site adjustment of process parameters and electrical control parameters to suppress torsional vibration.

1. Introduction

The torsional vibration of the main drive system of the rolling mill is one of the common rolling mill vibration phenomena. In field production, torsional vibration often leads to unstable rolling, which affects the surface quality of the strip and damage to the drive parts. The research method of rolling mill torsional vibration is to simplify the drive system into a multi-inertia torsional vibration model, establish the corresponding linear or nonlinear dynamic equation, and then study the vibration characteristics of the system according to the mathematical model.

In terms of modelling methods, most of the literatures establish nonlinear dynamic models and use nonlinear theory to solve the vibration characteristics of the system, but the nonlinear factors considered are different. First, Peng et al. [1] established a nonlinear dynamic model of the transmission system under the eccentric excitation of the rotating shaft, and concluded that the energy input caused by the eccentricity would lead to the instability of the rolling interface. Shen et al. [2] calculated the chaotic dynamic response of rolling mill drive system under the excitation of gap collision. Shi et al. [3–5] considered the nonlinear factors such as stiffness, friction damping, and clearance of the rolling mill transmission system and obtained the amplitude-frequency characteristic equation and bifurcation response equation of the system. Amer et al. [6] established a one-degree-of-freedom nonlinear dynamic equation based on the characteristics of the universal joint shaft of the rolling mill and solved the frequency response characteristics of the system. Chen and Li [7] studied the effect of rolling lubrication on the torsional vibration of rolling mills.

In considering the nonlinear content of the main drive system of the rolling mill, in addition to the nonlinear factors existing in the drive system mentioned above, there are many literatures that study the coupled nonlinear characteristics of the drive system of the rolling mill. Peng et al. [8] found that the vibration of the rolling mill roll has the nature of coupled vibration, and the rolling mill parameters have a great influence. Gao et al. [9] established a nonlinear vibration model of the coupling between the main drive mechanical system of the rolling mill and the strip and obtained the amplitude-frequency characteristics of the coupled vibration and its influencing factors. Sun et al. [10] established a torsional vibration mechanical model of a six-high rolling mill and studied the relationship between the

rolling process parameters and the torsional vibration of the roll system. Hou et al. [11] established a vertical-torsional coupling dynamics model of a four-high rolling mill and studied the amplitude-frequency response characteristics and bifurcation behavior of the system. Liu et al. [12–15] established a strong nonlinear electromechanical coupled torsional vibration model based on a salient-pole synchronous motor and DC motor and analyzed the influence of electrical and mechanical parameters on the rolling mill torsional vibration. Liu et al. [16] established a rolling mill-electric coupling torsional vibration model driven by a DC motor and studied the bifurcation and chaotic phenomena of the system. Zhang et al. [17, 18] established a nonlinear model of rolling mill-electric coupling based on AC motor and studied the influence of the rotor induced current and electrical parameters on the torsional vibration of the main drive system. Zhang et al. [19] studied the influence characteristics of rolling mill drive system time delay on nonlinear vibration.

Aiming at the torsional vibration problem of the main drive system of the F5 rolling mill of a steel mill, this paper establishes a multiphysics coupled linear dynamic model of the main drive of the rolling mill, the rolling strip, and the main motor control system. The control system block diagram, the linear dynamic equation, and the torsional vibration model are transformed into each other, and the coupling mechanism and influence law of the system are more intuitively and clearly described. The specific research contents are arranged as follows: in Section 2, the five-inertia torsional vibration model of the main drive mechanical system of the rolling mill is established. In Section 3, the coupled dynamic equations and torsional vibration model of the strip and main drive system are established. In Section 4, the control block diagram, dynamic equation, and torsional vibration model of the coupling of the motor control system and the main drive system are established. In Section 5, a multiphysics coupled torsional vibration model of the main drive system of the rolling mill is established. In Section 6, the natural frequencies of the main drive system of the rolling mill under various operating conditions are simulated and an example of torsional vibration suppression by changing the natural frequency is given. The conclusion is given in Section 7.

2. Torsional Vibration Mechanical Model of Rolling Mill Main Drive System in Shutdown State

The mechanical structure of the main drive system of F5 cold-rolling mill in a steel plant is shown in Figure 1. The rolling mill is a six-high rolling mill, and the upper and lower work rolls are the driving rolls. The main motor drove the gear box power. The motor and gearbox were connected by an arc tooth joint. The upper and lower shafts of the gearbox were driven at a ratio of 1 : 1. The cross-universal joint shaft is used for torque transmission between the gearbox and work roll.

Considering only the main force-bearing components, the main drive system is simplified to a five-inertia torsional vibration model, and the friction between work rolls and middle rolls is equivalent to damping c_{5wmd} and c_{5wmu} to the ground. The torsional vibration model in the free state was simplified as shown in Figure 2.

According to Figure 2, the vibration differential equations are established for each component, and the vibration differential equations of the main drive system are obtained as follows:

$$J_{5m}\ddot{\varphi}_{5m} + c_{5mj}\dot{\varphi}_{5m} - c_{5mj}\dot{\varphi}_{5jd} + k_{5mj}\varphi_{5m} - k_{5mj}\varphi_{5jd} = 0, \tag{1}$$

$$\begin{aligned} J_{5jd}\ddot{\varphi}_{5jd} - c_{5mj}\dot{\varphi}_{5m} + \left(c_{5mj} + c_{5jud} + c_{5jwd}\right)\dot{\varphi}_{5jd} - c_{5jud}\dot{\varphi}_{5ju} - c_{5jwd}\dot{\varphi}_{5wd} \\ - k_{5mj}\varphi_{5m} + \left(k_{5mj} + k_{5jud} + k_{5jwd}\right)\varphi_{5jd} - k_{5jud}\varphi_{5ju} - k_{5jwd}\varphi_{5wd} = 0, \end{aligned} \tag{2}$$

$$\begin{aligned} J_{5ju}\ddot{\varphi}_{5ju} - c_{5jud}\dot{\varphi}_{5jd} + \left(c_{5jud} + c_{5jwu}\right)\dot{\varphi}_{5ju} - c_{5jwu}\dot{\varphi}_{5wu} - k_{5jud}\varphi_{5jd} + \\ \left(k_{5jud} + k_{5jwu}\right)\varphi_{5ju} - k_{5jwu}\varphi_{5wu} = 0, \end{aligned} \tag{3}$$

$$J_{5wd}\ddot{\varphi}_{5wd} - c_{5jwd}\dot{\varphi}_{5jd} + \left(c_{5jwd} + c_{5wmd}\right)\dot{\varphi}_{5wd} - k_{5jwd}\varphi_{5jd} + k_{5jwd}\varphi_{5wd} = 0, \tag{4}$$

$$J_{5wu}\ddot{\varphi}_{5wu} - c_{5jwu}\dot{\varphi}_{5ju} + \left(c_{5wmu} + c_{5jwu}\right)\dot{\varphi}_{5wu} - k_{5jwu}\varphi_{5ju} + k_{5jwu}\varphi_{5wu} = 0. \tag{5}$$

Here, J_{5m}, J_{5jd}, J_{5ju}, J_{5wd}, and J_{5wu} are the equivalent rotational inertia of the motor rotor, lower gear shaft, upper gear shaft, lower work roll, and upper work roll; φ_{5m}, $\dot{\varphi}_{5m}$, and $\ddot{\varphi}_{5m}$ are the torsional vibration angle, angular velocity, and angular acceleration of the motor rotor, respectively; φ_{5jd}, $\dot{\varphi}_{5jd}$, and $\ddot{\varphi}_{5jd}$ are the torsional vibration angle, angular velocity, and angular acceleration of the lower gear shaft, respectively; φ_{5ju}, $\dot{\varphi}_{5ju}$, and $\ddot{\varphi}_{5ju}$ are the torsional vibration angle, angular velocity, and angular acceleration of the upper gear shaft, respectively; φ_{5wd}, $\dot{\varphi}_{5wd}$, and $\ddot{\varphi}_{5wd}$ are the torsional vibration angle, angular velocity, and angular acceleration of the lower work roll, respectively; φ_{5wu}, $\dot{\varphi}_{5wu}$, and $\ddot{\varphi}_{5wu}$ are the torsional vibration angle, angular velocity, and angular acceleration of the upper work roll, respectively; c_{5mj}, c_{5jud},

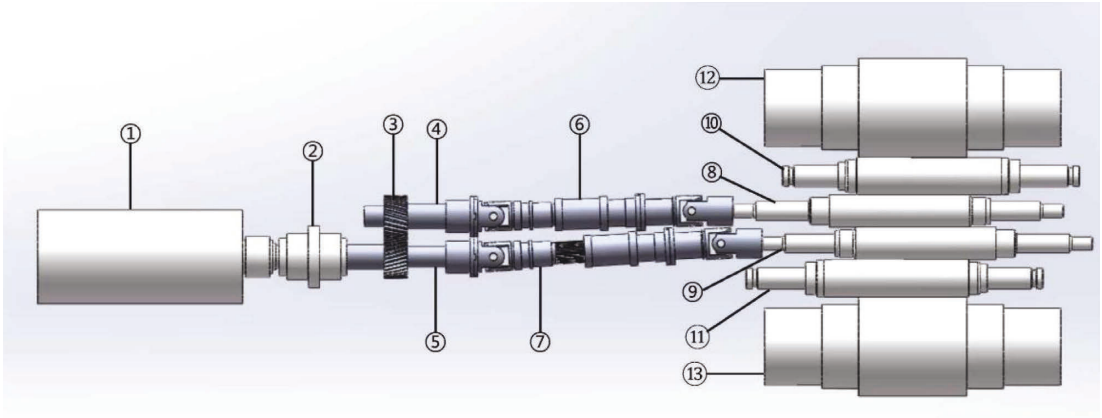

Figure 1: Mechanical structure diagram of the main drive system of F5 rolling mill. ① The motor rotor. ② Arc toothed shaft. ③ Meshing gear. ④ Upper gear shaft. ⑤ Lower gear shaft. ⑥ Upper universal joint shaft. ⑦ Lower universal joint shaft. ⑧ Upper work roll. ⑨ Lower work roll. ⑩ Upper intermediate roller. ⑪ Lower intermediate roller. ⑫ Upper support roller. ⑬ Lower support roller.

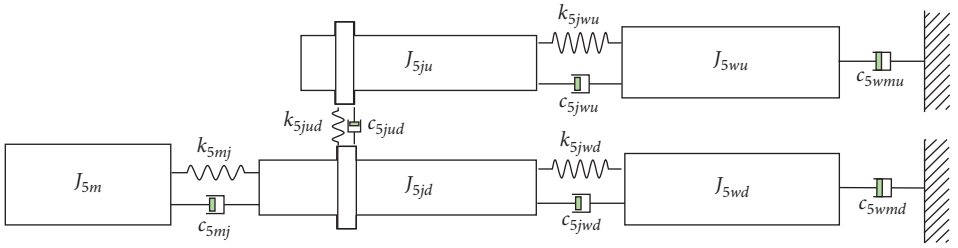

Figure 2: Model diagram of the torsional vibration of F5 rolling mill main drive system in a free state.

c_{5jwd}, and c_{5jwu} are the equivalent structural damping of the arc toothed shaft, meshing gears, lower universal joint shaft, and upper universal joint, respectively, and the damping ratio is 0.005; c_{5wmd} is the equivalent friction damping between lower work roll and lower intermediate roll; c_{5wmu} is the equivalent friction damping between upper work roll and upper intermediate roll; k_{5mj}, k_{5jud}, k_{5jwd}, and k_{5jwu} are the equivalent stiffness of the arc toothed shaft, meshing gears, lower universal joint shaft, and upper universal joint, respectively.

By viewing the drawings of the field equipment and calculating the equivalent of the model, the equivalent parameters of the model are set as shown in Table 1, and the damping ratio in the model is set to 0.01.

3. Mechanical Model of Torsional Vibration under the Influence of Strip Steel in the Main Drive System of Rolling Mill

3.1. Rolling Moment Model. For the convenience of analysis, the following assumptions were made for the rolling state:

(1) n the rolling deformation zone, the friction coefficients of the upper and lower work rolls and strip were equal and constant

(2) In the rolling deformation area, the unit positive pressure of the upper and lower work rolls and the strip is evenly distributed and directed towards the axis

(3) The friction and positive pressure conformed to Coulomb's law of friction.

(4) The rolled pieces did not broaden

The rolling deformation zone can be divided into back-slip area and forward-slip area [20]. The speed of the rollers in the back-slip area is higher than the speed of the strip, and the rollers drive the strip forward. The state is opposite in the forward-slip area.

The friction torque acting on the work roll can be expressed as follows:

$$M = \frac{(T_1 - T_2)D}{2}, \tag{6}$$

where T_1 denotes friction force in the back-slip area and can be described as follows:

$$T_1 = \frac{\mu \overline{p} B(\alpha - \gamma)D}{2}. \tag{7}$$

T_2 denotes the friction force in the forward-slip area and can be described as follows:

$$T_2 = \frac{\mu \overline{p} B\gamma D}{2}. \tag{8}$$

Here μ denotes friction coefficient between work roll and strip; $\overline{p}$ denotes unit positive pressure of work roll and strip; B denotes strip width; D denotes work roll diameter; and α denotes the strip bite angle and can be described as follows:

Table 1: Equivalent parameters of rotational inertia and stiffness for the main drive system.

Parameter	Value	Unit
J_{5m}	135.66	kg · m^2
J_{5jd}	57.5	kg · m^2
J_{5ju}	52.9	kg · m^2
J_{5wd}	79.2	kg · m^2
J_{5wu}	79.2	kg · m^2
k_{5mj}	7690000	N · m/rad
k_{5jud}	5170000	N · m/rad
k_{5jwd}	3580000	N · m/rad
k_{5jwu}	3580000	N · m/rad

$$\alpha \approx \sqrt{\frac{2\Delta h}{D}}. \tag{9}$$

Here, Δh denotes deformation of strip thickness; and γ denotes neutral angle in the roll-strip interface.

According to the principle of equal second flow of metal in the deformation zone, equations (10)–(12) are established:

$$v_\gamma h_\gamma = v_1 h_1, \tag{10}$$

$$v_\gamma = v\cos\gamma, \tag{11}$$

$$h_\gamma = h_1 + D(1-\cos\gamma). \tag{12}$$

The Fink forward-slip formula is shown in the following equation:

$$\begin{aligned} f &= \frac{v_1 - v}{v}, \\ &= \frac{v_1}{v} - 1, \\ &= \frac{h_\gamma \cos\gamma}{h_1} - 1, \\ &= \frac{[h_1 + D(1-\cos\gamma)]\cos\gamma}{h_1} - 1, \\ &= \frac{(D\cos\gamma - h_1)(1-\cos\gamma)}{h_1}. \end{aligned} \tag{13}$$

Since γ is small, we can set $\cos\gamma \approx 1$ and $1-\cos\gamma \approx \gamma^2/2$, and $D \gg h_1$. Therefore, (14) and (15) can be obtained as follows:

$$f = \frac{(D-h_1)\gamma^2}{2h_1} \approx \frac{D\gamma^2}{2h_1}, \tag{14}$$

$$\gamma = \sqrt{\frac{2h_1(v_1 - v)}{Dv}}. \tag{15}$$

Here, v_h denotes strip exit speed; h_1 denotes strip outlet thickness; and v denotes work roll line speed and can be described as follows:

$$v = \frac{\dot\varphi D}{2}. \tag{16}$$

Here, $\dot\varphi$ denotes work roll angular velocity;

Substituting equations (7)–(9) and (8) into (6), we can obtain the following equation:

$$M = \frac{\mu\overline{p}BD^2}{4}\left(\sqrt{\frac{2\Delta h}{D}} - 2\sqrt{\frac{2h_1(v_h - v)}{Dv}}\right). \tag{17}$$

By combining (17) with (16) after the Taylor expansion, without considering the steady-state rolling torque, the linearized torque fluctuations ΔM_{5wu} and ΔM_{5wd} of the upper and lower work rolls under the torsional vibration can be obtained, as shown in the following equations:

$$\Delta M_{5wd} = c_{5wd}\dot\varphi_{5wd}. \tag{18}$$

$$\Delta M_{5wu} = c_{5wu}\dot\varphi_{5wu}. \tag{19}$$

Here, c_{5wd} and c_{5wu} are the rolling damping between the lower and upper work roll and strip; c_{5wd} and c_{5wu} can be represented by equations (20) and (21), respectively,

$$c_{5wd} = \frac{\mu\overline{p}BD_{5wd}^3\sqrt{2h_1}}{8\sqrt{D\left(v_1 v^3 - v^4\right)}}, \tag{20}$$

$$c_{5wu} = \frac{\mu\overline{p}BD_{5wu}^3\sqrt{2h_1}}{8\sqrt{D\left(v_1 v^3 - v^4\right)}}. \tag{21}$$

The sizes of c_{5wd} and c_{5wu} are related to the rolling material, size of the strip, and friction state. The specifications and rolling parameters of typical SPCC strips are shown in Table 2.

3.2. Asynchronous Rolling Model. The function of the rolling torque on the rotational speed of the rolls was previously established. When the rotational speed decreased, the rolling torque decreased, whereas when the rotational speed increased, the rolling torque also increased.

The rolling experiment was carried out on a single-stand cold-rolling mill driven by a double motor in a factory. First, the rolling speed of the upper work roll was kept constant, the rolling speed of the lower work roll was increased and decreased, and the output torque of the upper and lower motors was recorded, respectively. Then, the rolling speed of the lower work roll was kept unchanged, the rolling speed of the upper work roll was increased and decreased, and also the output torque of the upper and lower motors was recorded. The rolling parameters of the fifth pass of this rolling mill are basically the same as those of the F5 cold-rolling mill, and the experimental data are shown in Figures 3 and 4.

It can be found that the rolling torque is not only related to the speed of the own roll but also related to the speed of the other roll. For example, as shown in Figure 3, when the speed of the upper work roll is kept constant and the speed of the lower work roll is changed, the motor torque driving the lower work roll increases or decreases proportionally with the rotation speed, and the motor torque driving the upper

Table 2: Typical strip rolling parameters.

Parameter	Value	Unit
μ	0.05	
$\overline{p}$	900	Mpa
B	1000	mm
D	400	mm
Δh	0.05	mm
v	1200	m/min
v_h	1210	m/min
h_1	0.5	mm

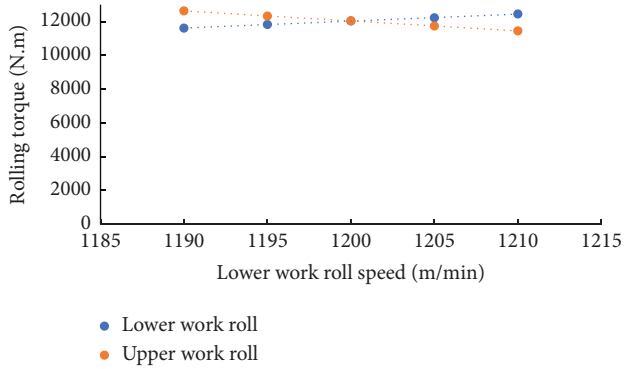

Figure 3: The relationship between the rolling torque of the upper and lower work rolls and the rolling speed of the lower work roll.

work roll changes in the opposite direction. This shows that when the rotational speed of the upper and lower work rolls is different and the asynchronous rolling phenomenon occurs, the asynchronous rolling between the rolls will generate additional torque.

When the torsional vibration of the upper and lower work rolls of the F5 cold-rolling mill occurs, an additional torque of asynchronous rolling will also be generated owing

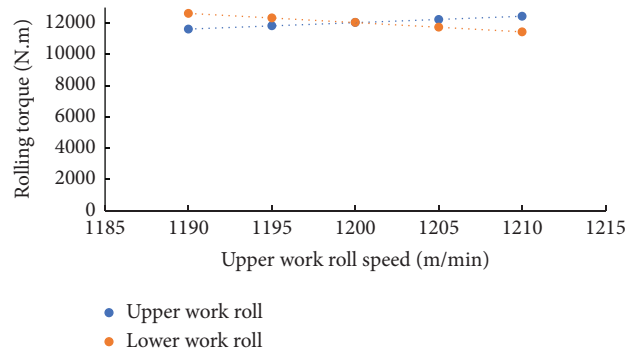

Figure 4: The relationship between the rolling torque of the upper and lower work rolls and the rolling speed of the upper work roll.

to the difference in amplitude and phase. The magnitude of the additional torque is positively correlated with the speed difference between the upper and lower work rolls; therefore, the additional torque can be expressed as follows:

$$\Delta M_{\dot{\varphi}} = c_{5wdu}\left(\dot{\varphi}_{5wd} - \dot{\varphi}_{5wu}\right). \tag{22}$$

Here, c_{5wdu} represents the additional damping of asynchronous rolling, and the value is 1.5 times the rolling damping value.

3.3. Work Roll Torsional Vibration Differential Equation. Considering the external force on the work roll under the influence of the strip, the rolling torque and additional torque are increased compared to the free state and are introduced into the vibration differential in equations (4) and (5) of the upper and lower work rolls, respectively. The torsional vibration equation of the work rolls in the rolling state becomes as shown in the following equations:

$$\begin{aligned} J_{5wd}\ddot{\varphi}_{5wd} - c_{5jwd}\dot{\varphi}_{5jd} + \left(c_{5jwd} + c_{5wdu} + c_{5wd} + c_{5wmd}\right)\dot{\varphi}_{5wd} - c_{5wdu}\dot{\varphi}_{5wu} \\ - k_{5jwd}\varphi_{5jd} + k_{5jwd}\varphi_{5wd} = 0, \end{aligned} \tag{23}$$

$$\begin{aligned} J_{5wu}\ddot{\varphi}_{5wu} - c_{5jwu}\dot{\varphi}_{5ju} - c_{5wdu}\dot{\varphi}_{5wd} + \left(c_{5wdu} + c_{5wu} + c_{5jwu} + c_{5wmu}\right)\dot{\varphi}_{5wu} \\ - k_{5jwu}\varphi_{5ju} + k_{5jwu}\varphi_{5wu} = 0. \end{aligned} \tag{24}$$

The mechanical models corresponding to the torsional vibration differential equations (1)–(2), (3), and (24) are shown in Figure 5.

Compared with the free state, the main drive system has a torsional vibration model under the influence of the strip, which increases the rolling damping constraint, as well as the additional damping constraint for asynchronous rolling between the upper and lower work rolls. The damping size was determined by the rolling process parameters.

4. Mechanical Model of the Torsional Vibration of Rolling Mill Main Drive System to Simulate Rolling State

Simulated rolling is to remove the strip in the roll gap, the same rolling force was applied through the rolling mill pressing system, and the main motor was run at the same speed to conduct the dynamic pressing test. The main motor of the on-site rolling mill adopts the double closed-loop

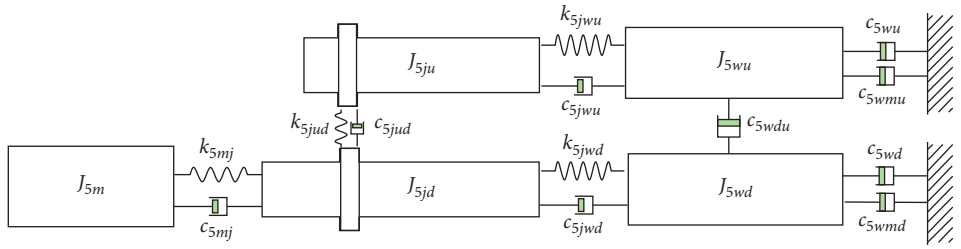

Figure 5: Model of the torsional vibration under the influence of strip steel in the main drive system of F5 rolling mill.

control mode of speed loop and current loop, the speed loop is PID (proportional integral derivative) control, and the current loop is P (proportional) controller. This control method has mature technology, high reliability, and good stability, which is convenient for mode switching and parameter adjustment.

In the simulated rolling experiment, the torsional vibration response amplitude of 26.5 Hz obtained by the torque sensor installed on the motor output shaft is shown in Figure 6, by switching the control mode of the main motor.

When the main motor adopts different speed regulation methods, the torsional vibration response of the motor shaft is also different. In order to explain the torsional vibration phenomenon in Figure 6 clearly, it is necessary to establish the electromechanical coupling torsional vibration model of the main drive system under different control modes.

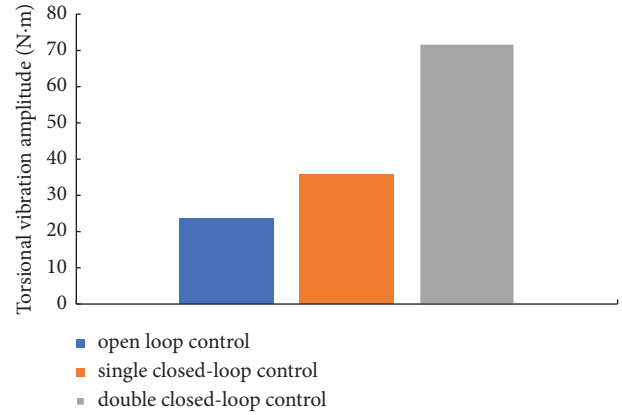

Figure 6: Torsional vibration response amplitude of the main motor output shaft.

4.1. Torsional Vibration Model When Motor Speed Is Open-Loop Controlled. Although AC asynchronous motors and DC motors have different structures, the vector control technology of the rotor flux linkage orientation adopted in the field enables AC and DC motors to have the same torque control characteristics, and the transfer functions are similar. To study this more intuitively, the following uses an equivalent DC motor [21].

The instantaneous voltage balance equation of the DC motor is given by the following equation:

$$U_5 = E + I_d R + L\frac{\mathrm{d}I_d}{\mathrm{d}t}. \tag{25}$$

Here, U_5 denotes the given voltage keeping constant of the motor; R denotes the motor armature resistance; L denotes the motor armature inductance; E denotes the induced electromotive force of armature and can be described as follows:

$$E = C_e\omega_{5m}. \tag{26}$$

Here, C_e denotes motor induced electromotive force coefficient; ω_{5m} denotes the instantaneous angular velocity of the motor rotor and can be described as follows:

$$\omega_{5m} = \omega_{5m0} + \Delta\omega_{5m}. \tag{27}$$

Here, ω_{5m0} denotes motor steady-state angular velocity; $\Delta\omega_{5m}$ denotes motor dynamic angular velocity;

I_d is the motor instantaneous current and can be described as follows:

$$I_d = I_{d0} + \Delta I_d. \tag{28}$$

Here, I_{d0} denotes motor steady-state current; ΔI_d denotes dynamic fluctuation of motor current.

Combining equations (25)–(28), when the motor has no torque fluctuation or speed fluctuation, the static voltage balance equation of the motor is given as follows:

$$U_5 = C_e\omega_{5m0} + I_{d0}R. \tag{29}$$

By combining (25) with (29), the dynamic voltage balance equation of the motor is shown as follows:

$$0 = C_e\Delta\omega_{5m} + \Delta I_d R + L\frac{\mathrm{d}\Delta I_d}{\mathrm{d}t}. \tag{30}$$

In addition, the dynamic torque of the motor is given as follows:

$$\Delta T_{5e} = C_t\Delta I_d. \tag{31}$$

where C_t is the motor induction torque coefficient.

Without considering the rigid rotation of the traditional system, where $\Delta\omega_{5m} = 30/\pi\dot{\varphi}_{5m}$ and $T_e = L/R$ are defined, combining the equations (30) and (31) and equation (5) can obtain the open-loop control dynamic system of the motor speed. The transmission block diagram is shown in Figure 7.

In Figure 5, T_e is the electromagnetic time constant of the motor, because $T_e \ll 1$, the inertia link of the motor can be treated as a proportional link. Here, $c_{5me} = 30C_eC_t/\pi R$ is defined, and ignoring T_e, the transfer block diagram of the rotor is equivalently transformed into a torsional vibration differential equation, as shown in the following equation:

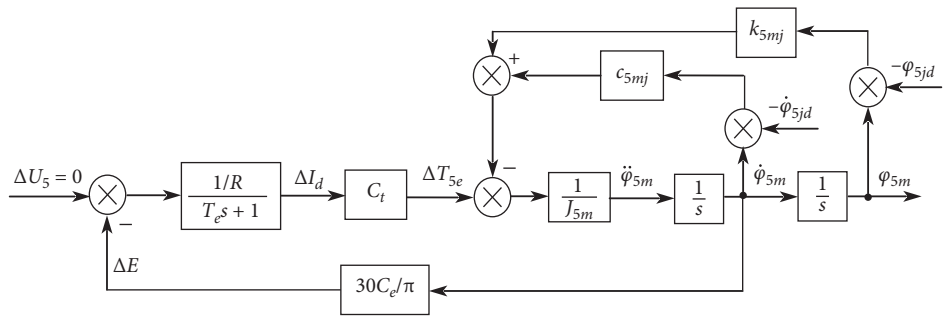

Figure 7: Block diagram of the electromechanical coupling system of the motor rotor in the motor open-loop control mode.

$$J_{5m}\ddot{\varphi}_{5m} + \left(c_{5mj} + c_{5me}\right)\dot{\varphi}_{5m} - c_{5mj}\dot{\varphi}_{5jd} + k_{5mj}\varphi_{5m} - k_{5mj}\varphi_{5jd} = 0. \tag{32}$$

where c_{5me} denotes the electromagnetic damping of the motor.

The mechanical models corresponding to the torsional vibration differential equations (2)–(3) 45 and (32) are shown in Figure 8.

From another aspect, the mechanical characteristic curve of the motor is shown in Figure 9, without considering the steady-state torque and steady-state speed. The fluctuating electromagnetic torque is always in the opposite direction to the fluctuating speed, and its magnitude changes proportionally. The dynamic effect of an open-loop control motor is similar to a damper.

In summary, the electromagnetic effect of the motor is equivalent to increasing the damping constraint of the motor rotor to the ground, when the electromagnetic torque is regarded as the external force of the mechanical system. The damping value is determined by the motor parameters. The motor and inverter nameplate parameters are shown in Table 3. Compared with the model in Figure 2, the above model has the same moment of inertia and torsional stiffness, but only changes the constraint conditions of the motor rotor, which affects the natural frequency of the system.

$C_e = 2.3$ and $C_t = 31.515$ are obtained by the following equations:

$$\begin{aligned} P_5^* &= U_5^* I_5^*, \\ U_5^* &= E_5^* + RI_5^*, \\ E_5^* &= C_e \omega_5^*, \\ T_{5e}^* &= 9550P* /\omega*, \\ T_{5e}^* &= C_t I_5^*. \end{aligned} \tag{33}$$

4.2. Torsional Vibration Model When the Motor Adopts Speed Single Closed-Loop Control. The control mode of the main motor is switched to the speed single closed-loop control mode, and the speed controller adopts the proportion-integration (PI) control mode. The dynamic single-closed-loop motor speed control block diagram, which does not consider the static control component, is shown in Figure 10.

Here, $c_{5mk} = K_p K_s C_t / R$ and $k_{5mk} = K_s C_t / RT_n$ are defined; converting the control block diagram to a differential equation is shown as follows:

$$\begin{aligned} J_{5m}\ddot{\varphi}_{5m} + \left(c_{5mj} + c_{5me} + c_{5mk}\right)\dot{\varphi}_{5m} - c_{5mj}\dot{\varphi}_{5jd} \\ + \left(k_{5mj} + k_{5mk}\right)\varphi_{5m} - k_{5mj}\varphi_{5jd} = 0, \end{aligned} \tag{34}$$

where c_{5mk} denotes the damping of the single closed-loop control of the motor, k_{5mk} denotes the stiffness of the single closed-loop control of the motor, K_p is the proportional control parameter, T_n is the integral control parameter, and K_s is the power amplifier magnification.

The mechanical models corresponding to the torsional vibration differential equations (2)–(3) (4) (5) and (34) are shown in Figure 11.

In Figure 10, the electromagnetic torque generated by the motor is not only affected by the mechanical characteristics of the motor but also related to the PI controller of the speed loop, when the main motor adopts the speed single closed-loop control system. When the speed fluctuates, the P controller controls the motor to also generate a reverse proportional electromagnetic torque. Compared with the open-loop state, the mechanical properties of the motor are improved in hardness. The I controller makes the motor to generate an electromagnetic torque, that is, inversely proportional to the torsion angle, and the dynamic effect is similar to a torsion spring. Through the comprehensive analysis of Figures 10 and 11 and equation (34), it is equivalent to adding damping constraints and stiffness constraints to the motor rotor in the torsional vibration model, when the motor adopts a single closed-loop speed feedback control. The value of c_{5me} is determined by the performance parameters of the motor, which is a constant in the model. c_{5mk} is determined by the proportional control parameters and motor parameters, and its size can be changed by adjusting the proportional control parameters; k_{5mk} is determined by the integral control parameters and motor parameters, and its size can also be changed by adjusting the integral control parameters.

4.3. Torsional Vibration Model When the Motor Adopts Double Closed-Loop Speed Control. When the control mode of the main motor is switched to double closed-loop speed control, the dynamic control structure is shown in Figure 12. The inner loop is the current loop, which uses the

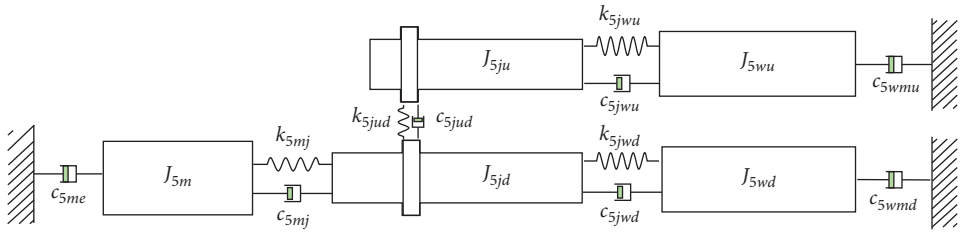

Figure 8: Torsional vibration model of the main drive system of the F5 rolling mill considering the action of the motor.

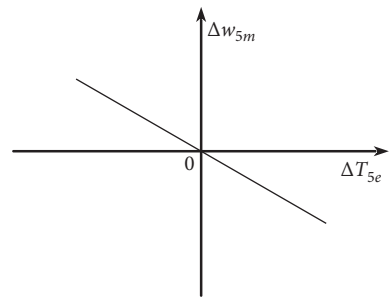

Figure 9: The mechanical characteristic curve of the motor to remove the steady-state component.

Table 3: Motor electrical parameters.

Name	Parameter	Value	Unit
Rated voltage	P_5^*	3300	kW
DC voltage	U^*	3300	V
Rated speed	$\omega_5^{*_5}$	1000	r/min
Equivalent resistance	R	1	Ω
Equivalent inductance	L	9.4	mH

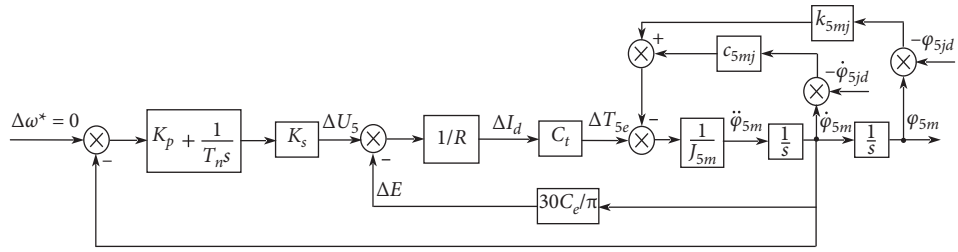

Figure 10: Block diagram of the rotor electromechanical coupling system under single closed-loop control of motor speed.

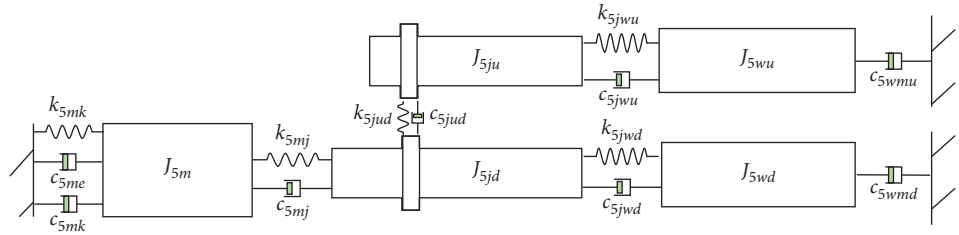

Figure 11: Torsional vibration model diagram under single closed-loop control of motor speed of the main drive system of F5 rolling mill.

proportional control mode; the outer loop is the speed loop, which uses the proportion-integration (PI) control mode and bypasses differential negative feedback.

Here, $J_{5mk} = T_d K_i K_s C_t/(K_i K_s + R)$, $c'_{5me} = C_e C_t/(K_i K_s + R)$, $c'_{5mk} = K_p K_i K_s C_t/(K_i K_s + R)$, and $k'_{5mk} = K_i K_s C_t/(K_i K_s + R)T_n$ are defined. Owing to $K_i K_s \gg R$, the above

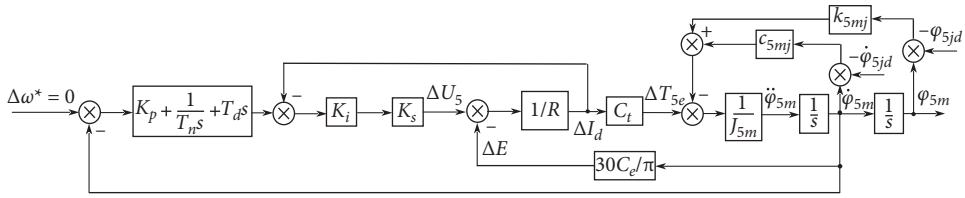

Figure 12: Block diagram of the electromechanical coupling system of motor rotor under double closed-loop control of motor speed.

formula can be simplified to $J_{5mk} = T_d C_t$, $c'^{5me} = C_e C_t/(K_i K_s)$, $c'_{5mk} = K_p C_t$, and $k'_{5mk} = C_t/T_n$.

Converting the control block diagram to a differential equation is shown as follows:

$$\begin{aligned}(J_{5m} + J_{5mk})\ddot{\varphi}_{5m} + \left(c_{5mj} + c'_{5me} + c'_{5mk}\right)\dot{\varphi}_{5m} \\ - c_{5mj}\dot{\varphi}_{5jd} + \left(k_{5mj} + k'_{5mk}\right)\varphi_{5m} - k_{5mj}\varphi_{5jd} = 0,\end{aligned} \tag{35}$$

where J_{5mk} denotes the motor double closed-loop control inertia, c'^{5me} denotes the motor double closed-loop electromagnetic damping, c'_{5mk} denotes the motor double closed-loop control damping, k'_{5mk} denotes the motor double closed-loop control stiffness, T_d is the derivative control parameter, and K_i is the current inner-loop proportional control parameter.

The mechanical models corresponding to the torsional vibration differential equations (2)–(5) and (35) are shown in Figure 13.

Compared with Figure 10, the current control loop in Figure 12 keeps the armature current of the motor as constant as possible, that is, the electromagnetic torque fluctuation becomes smaller. The electromagnetic torque change rates c'_{5me} and c'_{5mk} are both smaller than the value of the speed single closed-loop control state, which means that the hardness of the mechanical properties is reduced. The influence of the P and I parameters of the speed loop on the system is basically the same as that in the single closed-loop control mode. The speed differential control makes the motor to generate electromagnetic torque related to angular acceleration. The speed differential control parameters can change the equivalent moment of inertia of the motor rotor, through the dynamic equivalent conversion.

Combining Figures 12 and 13 and equation (35), the dynamic effect of the double closed-loop speed control mode on the motor can be equivalent to changing the damping, stiffness, and rotational inertia of the torsional vibration system in the torsional vibration mechanics model. c'_{5mk} and c'^{5me} are determined by the proportional control parameters of the outer and inner loops and the motor parameters, respectively, and their values can be changed by adjusting the proportional control parameters of the inner and outer loops; The values of k'_{5mk} and J_{5mk} are determined by the integral and differential control parameters of the outer loop, as well as the motor parameters, and can be adjusted by the integral and differential control parameters of the outer loop. By checking the control system parameters of the field device, the current parameter setting values are shown in Table 4.

5. Multiphysics Coupled Torsional Vibration Model under Rolling Conditions of the Main Drive System of the Rolling Mill

The field tests revealed that the main drive system of a rolling mill has different torsional vibration responses in the dynamic pressing and rolling states. To analyze the torsional vibration model under rolling conditions, it is necessary to consider the influence of the double closed-loop speed control system of the motor and the rolling load on the torsional vibration. The torsional vibration differential equations of the main drive system are given by equations (24), (25), (34), and (35), respectively.

The differential equation was transformed into a torsional vibration model, as shown in Figure 14.

6. Calculation and Analysis of the Natural Frequency of the Main Drive System of the F5 Rolling Mill

The torsional vibration differential equation of the main drive of the rolling mill established above has damping terms. Since it is difficult to calculate its natural frequency by the analytical method, the eigenvalue analysis module of the AMESim software is used to calculate the natural frequency of the main drive system under various working conditions. The multiphysics coupled equivalent torsional vibration model in the rolling state is shown in Figure 15.

6.1. Analysis of the Natural Frequency Variation of the Main Drive System of the Rolling Mill. The field data were introduced into the above model, and the natural frequencies in various states were calculated, as shown in Table 5.

By comparing the natural frequencies of each order in the down state with or without the influence of strip steel, and the double closed-loop control dynamic pressure state, and the actual rolling state, it can be observed that owing to the influence of rolling factors, the natural frequencies of the first two orders increase, the third order natural frequencies decrease, and the remaining orders remain unchanged.

By comparing the natural frequencies of each order in the down state and the open-loop control state of the motor, the second-order and fourth-order natural frequencies of the system increase most obviously, and the other orders do not change much.

By comparing the natural frequencies of each order in the single closed-loop and open-loop control states, the first-order natural frequency of the system increases significantly, and the rest of the natural frequencies decrease.

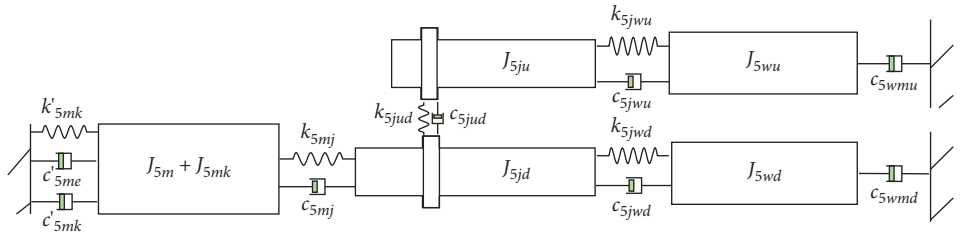

Figure 13: Model diagram of the torsional vibration under double closed-loop control of motor speed of the main drive system of F5 rolling mill.

Table 4: Motor control system parameters.

Parameter	K_p	K_s	K_i	T_n	T_d
Value	10	100	10	0.1	1

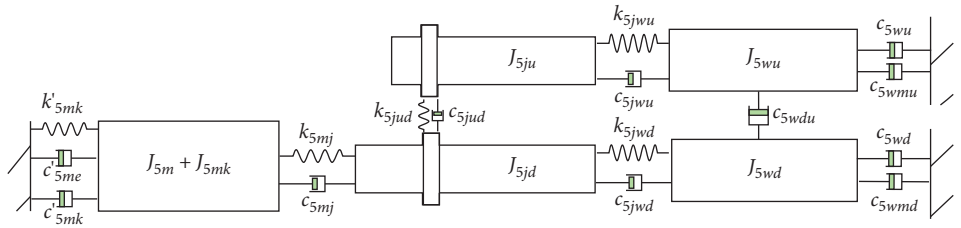

Figure 14: Considering the double closed-loop speed control system and the main drive torsional vibration model in rolling state simultaneously.

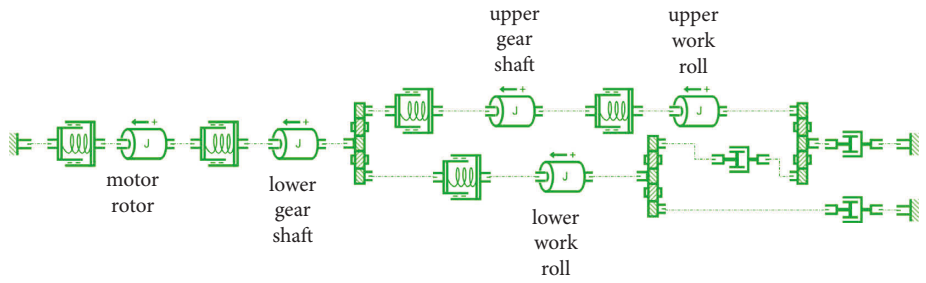

Figure 15: Multiphysics coupling equivalent torsional vibration AMESim simulation model of the main drive of rolling mill in rolling state.

Table 5: The natural frequency of the main drive system of the rolling mill under various conditions.

Natural frequency	Down state	Stop states considering strip influences	Motor open-loop control to simulate rolling	Motor single closed-loop control to simulate rolling	Motor double closed-loop control to simulate rolling	Rolling state
First order	0	0.4	0.3	17.1	0.14	0.46
Second order	26.9	27	29.5	27.6	26.5	26.6
Third order	35.2	35.1	35.2	29.8	34	33.8
Fourth order	62.7	62.7	64.5	62	62.3	62.3
Fifth order	96.2	96.2	96.3	95.8	95.7	95.7

By comparing the natural frequencies of each order in the double closed-loop control state and the single closed-loop control state, due to the reduction of the electromagnetic stiffness of the motor, the natural frequency of the first order is greatly reduced, and the impact on other orders is small.

In summary, the natural frequency of the main drive system of the rolling mill changes in different ways under

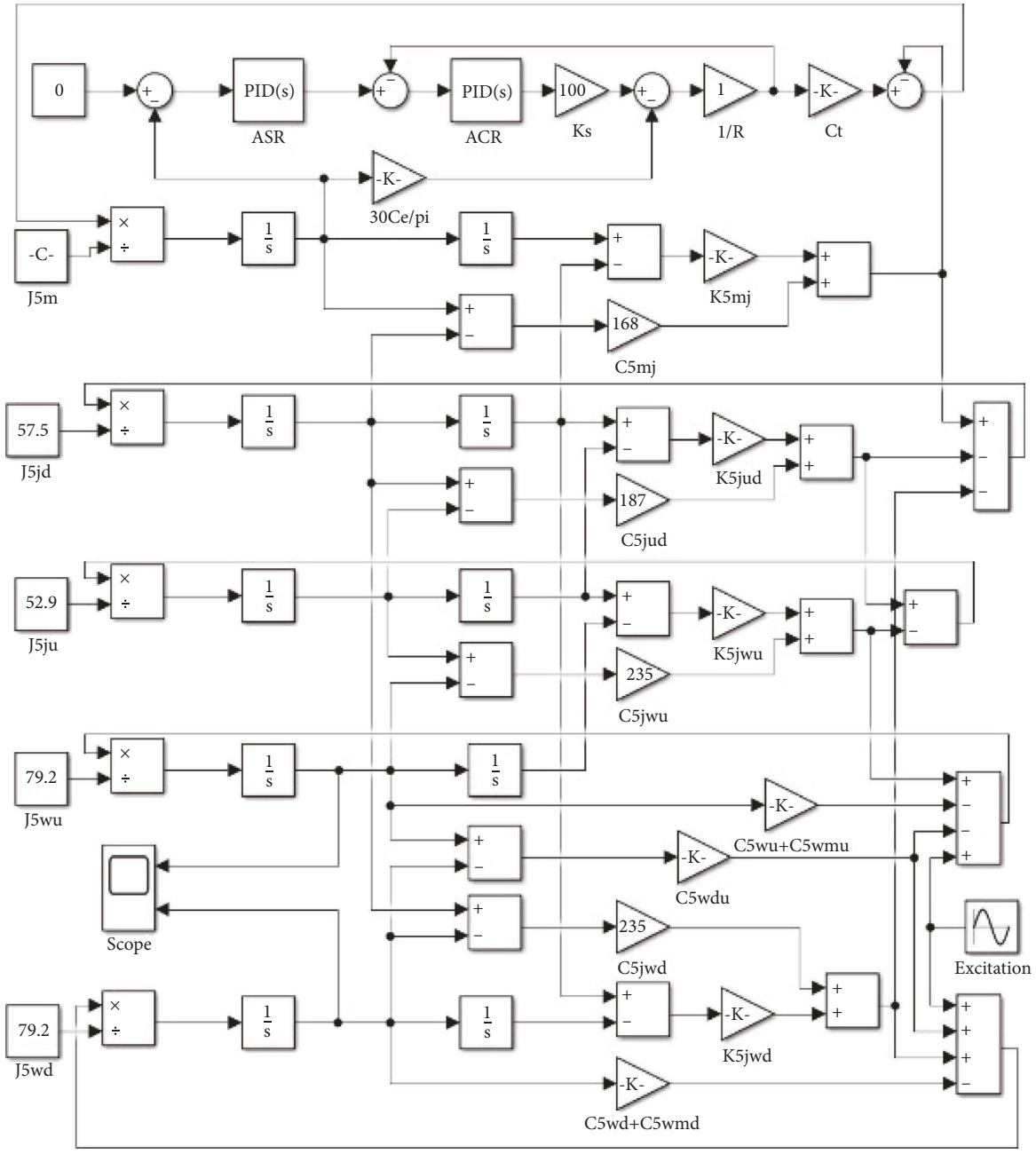

Figure 16: MATLAB/Simulink simulation diagram of the torsional vibration of the main drive system in the rolling state.

different conditions. Therefore, by adjusting the electrical control and rolling process parameters of the system, the natural frequencies of each stage of the main drive system of the rolling mill can be changed within a certain range around the original mechanical natural frequency. Directional guidance was provided to avoid the main driveline resonance caused by forced vibration.

6.2. Example Analysis of the Torsional Vibration Suppression. When rolling most high carbon steel grades, the rolling speed is 1000 m/min, and the rotation frequency of the drive system at this speed is as follows:

$$r = \frac{v}{60\pi D} = \frac{1000}{60 \times 0.4 \times \pi} = 13.3Hz. \quad (36)$$

Due to backlash and misalignment factors, torsional vibration excitations at twice the rotational frequency are formed in the transmission system. Figure 16 shows the MATLAB/Simulink simulation diagram of the torsional vibration of the main drive system in the rolling state established according to Figures 12 and 14.

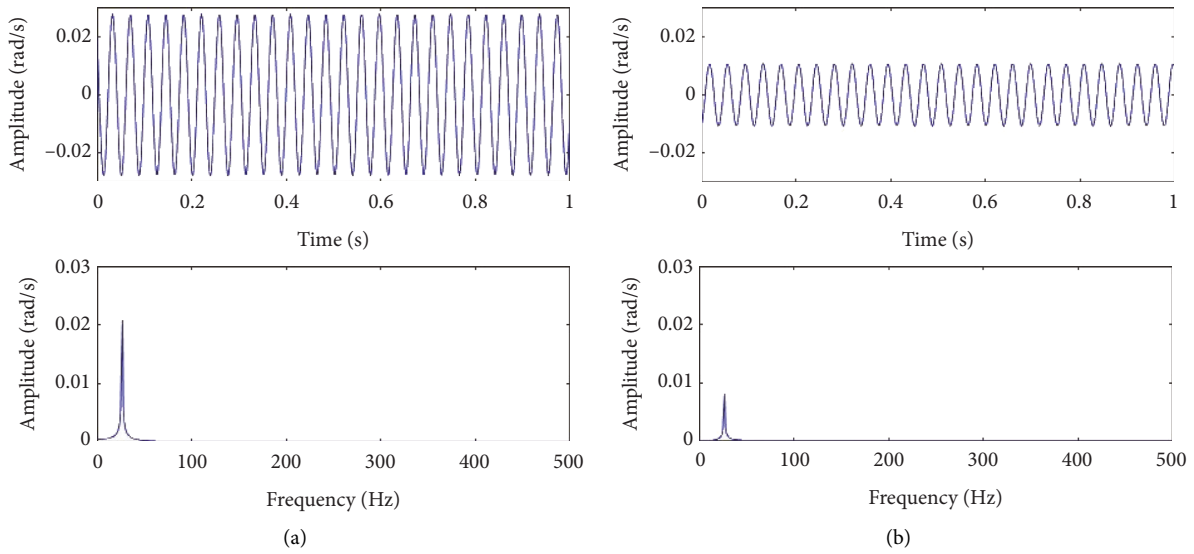

Figure 17: Spectrum diagram of torsional vibration response of upper (a) and lower (b) work rolls.

Table 6: Speed loop control parameter adjustment table.

Name	Initial setting value	Adjustment value
K_p	10	10
T_n	0.1	0.02
T_d	1	0

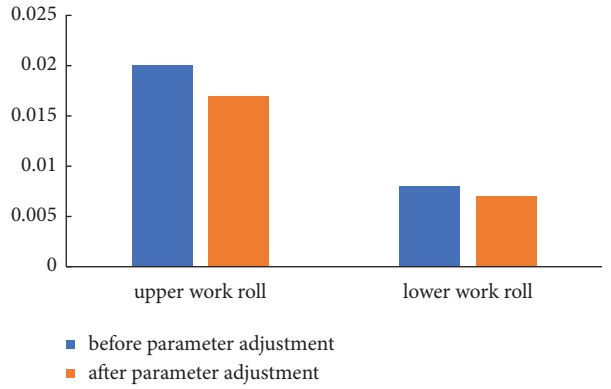

Figure 18: Comparison of the torsional vibration speed of upper and lower work rolls before and after vibration suppression.

As shown in Figure 16, the excitation applied to the rolls is $\Delta T = 100\sin(53.2\pi t)$, and the torsional vibration responses of the upper and lower work rolls are shown in Figure 17.

After comprehensive field tests, after adjusting the speed loop control parameters as shown in Table 6, the second-order natural frequency of the main drive system is changed from 26.6 Hz to 27 Hz, so that the excitation frequency is staggered from the natural frequency of the system to reduce the vibration amplitude, and the vibration suppression effect is shown in Figure 18.

The characteristic equation of the system is as follows:

$$\begin{aligned} D(s) = {} & J_{5wu}\left(J_{5m}R + J_{5m}K_iK_s + K_iK_sC_tT_d\right)T_n\pi s^3 + \\ & \cdot\left[\left(C_{5wu} + C_{5wmu}\right)\left(J_{5m}R + J_{5m}K_iK_s + K_iK_sC_tT_d\right)T_n\pi + J_{5wu}\left(30C_e + K_iK_sK_p\pi\right)C_tT_n\right]s^2 + \\ & \cdot\left[J_{5wu}K_iK_s\pi C_t + \left(C_{5wu} + C_{5wmu}\right)\left(30C_e + K_iK_sK_p\pi\right)C_tT_n\right]s + \left(C_{5wu} + C_{5wmu}\right)K_iK_s\pi C_t = 0. \end{aligned} \tag{37}$$

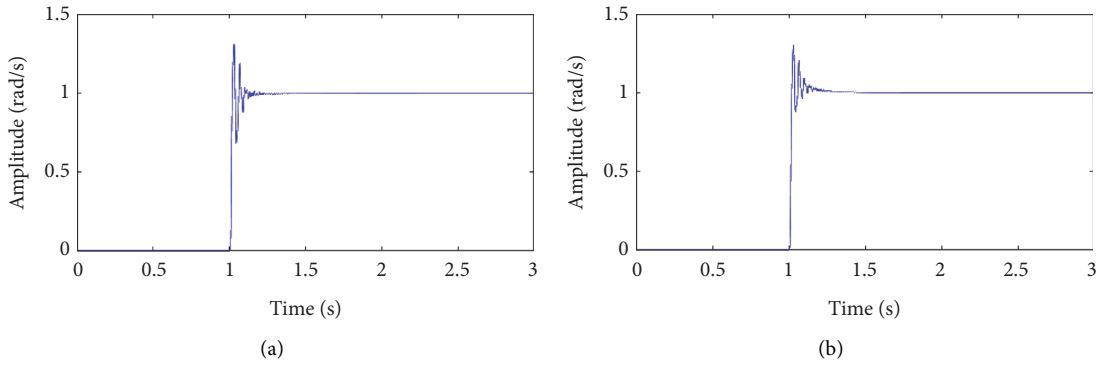

Figure 19: Upper work roll speed step response graph (a) Initial setting value; (b) Adjustment value.

After the parameters are adjusted, the eigenvalues of the system are -6.73, -1.164+3.2j, and -1.164-3.2j, respectively, and all the eigenvalues are negative real parts, indicating that the system is still stable.

Before and after the adjustment of the speed loop parameters in the main motor control system, the speed step response curve of the upper work roll is shown in Figure 19.

After the parameter adjustment, the speed step response of the upper work roll is more stable, indicating that this parameter adjustment scheme is feasible.

7. Conclusion

(1) The main drive system of a rolling mill is a multiphysics coupling system that includes a mechanical system, an electrical drive system, and a rolling interface. By determining the dynamic effects of the rolling torque and electromagnetic torque on the mechanical system as the boundary constraints on the mechanical system, the torsional vibration mechanical model and torsional vibration differential equations of the main drive system coupled with the mechanical-electrical-rolling interface multiphysics were established.

(2) The coupling mechanism of the rolling interface, electrical control system, and mechanical torsional vibration system was qualitatively analyzed by analyzing the influence of the rolling and control system parameters on the coefficients of the torsional vibration equations of the main drive system.

(3) The field parameters were substituted into the model to obtain the natural frequency of the main drive system under various modelling methods through analytical calculations. After comparison with the field test data, the calculated results were highly consistent with the field data, which verifies the correctness of the theory and the accuracy of the model. This provides a theoretical basis for adjusting the process parameters and motor control parameters on-site to suppress the torsional vibration of the main drive of the rolling mill.

Data Availability

The data used to support the findings of this study are available from the corresponding author upon request.

Conflicts of Interest

The authors declare that they have no conflicts of interest.

Acknowledgments

This research was supported by the National Natural Science Foundation of China (Grant no. 51775038).

References

[1] Y. Peng, J.-X. Cui, J.-L. Sun, and M. Zhang, "Torsional vibration for rolling mill with the drive system shaft axis deviations," *Arabian Journal for Science and Engineering*, vol. 46, no. 12, pp. 12165–12177, 2021.

[2] Y.-Z. Shen, H.-M. Liu, J. Xiong, and G.-J. Du, "Analysis of chaotic behavior of the main drive system with clearance of a heavey plate mill," *Engineering Mechanics*, vol. 27, no. 7, pp. 232–236, 2010.

[3] P.-M. Shi, J.-Z. Li, J.-S. Jiang, B. Liu, and D.-Y. Han, "Nonlinear dynamics of torsional vibration for rolling mill's main drive system under parametric excitation," *Journal of Iron and Steel Research International*, vol. 20, no. 1, pp. 07–12, 2013.

[4] P.-M. Shi, J.-Z. Li, D.-W. Zhao, and B. Liu, "Nonlinear torsional vibration dynamics of rolling mill's drive system under spindle angle parametric excitation," in *Proceedings of the 10th World Congress on Intelligent Control and Automation*, Beijing, China, July, 2012.

[5] P.-M. Shi, K.-W. Xia, B. Liu, and J.-S. Jiang, "Dynamics behaviors of rolling mill's nonlinear torsional vibration of multi-degree-of-freedom main drive system with clearance," *Journal of Mechanical Engineering*, vol. 48, no. 17, pp. 57–64, 2012.

[6] Y. A. Amer, A. T. El-Sayed, and F. T. El-Bahrawy, "Torsional vibration reduction for rolling mill's main drive system via negative velocity feedback under parametric excitation," *Journal of Mechanical Science and Technology*, vol. 29, no. 4, pp. 1581–1589, 2015.

[7] C. Chen and Y.-R. Li, "Influence of rolling lubrication on the self-excited vibration of rolling mill main drive system," *Journal of Vibration and Shock*, vol. 34, no. 16, pp. 161–165+182, 2015.

[8] R.-R. Peng, X.-Z. Zhang, and P.-M. Shi, "Coupled vibration behavior of hot rolling mill rolls under multinonlinear effects," *Shock and Vibration*, vol. 2020, Article ID 6104028, 14 pages, 2020.

[9] C.-Y. Gao, J.-X. Li, L. Liu, and L. Wei, "A nonlinear research on coupled vibration of strip steel with the impact of the main drive system of tandem mill," *Engineering Letters*, vol. 27, no. 3, pp. 441–446, 2019.

[10] J.-L. Sun, M. Zhang, and Y. Peng, "Torsional vibration of 6-h rolling mill based on continuum dynamics and its relationship with strip quality," *Engineering Mechanics*, vol. 31, no. 04, pp. 239–244, 2014.

[11] D.-X. Hou, D.-W. Guo, and X.-H. Chen, "A study on vertical-torsional coupled nonlinear vibration characteristics of 4-h rolling mill based on dynamic rolling force," *Journal of Vibration and Shock*, vol. 39, no. 20, pp. 106–112, 2020.

[12] S. Liu, X. Li, S.-S. Zhao, and H.-B. Li, "Bifurcation and chaos analysis of a nonlinear electromechanical coupling transmission system driven by AC asynchronous motor," *International Journal of Applied Electromagnetics and Mechanics*, vol. 47, no. 3, pp. 705–717, 2015.

[13] S. Liu, B.-P. Sun, S.-S. Zhao, J.-X. Li, and W.-M. Zhang, "Strongly nonlinear dynamics of torsional vibration for rolling mill's electromechanical coupling system," *Steel Research International*, vol. 86, no. 9, pp. 984–992, 2015.

[14] S. Liu, J.-J. Liu, Z. Wu, and J.-X. Li, "Bifurcation control for electromechanical coupling torsional vibration in rolling mill system driven by DC motor," *International Journal of Applied Electromagnetics and Mechanics*, vol. 50, no. 1, pp. 113–125, 2016.

[15] S. Liu, H.-L. Ai, B.-P. Sun, S. Li, and Z. Meng, "Bifurcation and chaos of electromechanical coupling main drive system with strongly nonlinear characteristic in mill," *Chaos, Solitons & Fractals*, vol. 98, pp. 101–108, 2017.

[16] H.-R. Liu, J.-J. Liu, F. Liu, Z. Zhu, K. Wang, and S. Liu, "Bifurcation and chaos for electromechanical coupling torsional vibration in rolling mill system driven by DC motor," *Journal of Vibroengineering*, vol. 18, no. 3, pp. 1920–1933, 2016.

[17] R.-C. Zhang and C.-L. Zhuo, "Parametrically excited vibration of electromechanical coupling system of a rolling mill main drive based on rotor induction current influence," *Journal of Vibration and Shock*, vol. 35, no. 17, pp. 1–6, 2016.

[18] R.-C. Zhang, Z. Gao, and Y.-Z. Ma, "Electromechanical coupling vibration characteristics of main drive system for rolling mill considering impacts of electrical parameters," *Mechanical Science and Technology for Aerospace Engineering*, vol. 35, no. 8, pp. 1189–1194, 2016.

[19] R. Zhang, J.-B. Wang, and L.-F. Ma, "Bifurcation analysis of a fractional-order delayed rolling mill's main drive electromechanical coupling system," *Advances in Mathematical Physics*, vol. 2021, Article ID 6358530, 10 pages, 2021.

[20] Q.-C. Jin, W.-H. Wang, R.-S. Jiang, L.-N.-S. Chiu, D. Liu, and W.-Y. Yan, "A numerical study on contact condition and wear of roller in cold rolling," *Metals*, vol. 7, no. 9, p. 376, 2017.

[21] C.-J. Li and W. Duan, *Electromechanical Vibration Control of Rolling Mill Drive AC Speed Regulation*, Metallurgical Industry Press, Beijing, China, 2003.

[22] C.-Y. Gao, G.-J. Du, R. Li, and X.-Q. Guo, "An analysis on strip vibration coupled with torsional vibration of main drive system of rolling mill," *Journal of Vibroengineering*, vol. 19, no. 8, pp. 5679–5690, 2017.

[23] Y.-K. Sun, *Model and Control of Hot and Cold Rolled Strip Mill*, Metallurgical Industry Press, vol. 36, no. 3, Beijing, China, 2010.